The American Journal of Pathology, Vol. 184, No. 3, March 2014

ELSEVIER

The American Journal of PATHOLOGY

ajp.amjpathol.org

SHORT COMMUNICATION

Primary Urethral Clear-Cell Adenocarcinoma

Comprehensive Analysis by Surgical Pathology, Cytopathology, and Next-Generation Sequencing

Rohit Mehra,*†‡ Pankaj Vats,*‡ Shanker Kalyana-Sundaram,*‡ Aaron M. Udager,* Michael Roh,* Ajjai Alva,†§ Jincheng Pan,‡¶ Robert J. Lonigro,†‡ Javed Siddiqui,‡ Alon Weizer,†‖ Cheryl Lee,†‖ Xuhong Cao,‡ Yi-Mi Wu,‡ Dan R. Robinson,‡ Saravana M. Dhanasekaran,‡ and Arul M. Chinnaiyan*†‡‖**

From the Departments of Pathology, Internal Medicine,§ and Urology‖ and the Comprehensive Cancer Center,† University of Michigan Health System, Ann Arbor, Michigan; the Michigan Center for Translational Pathology,‡ Ann Arbor, Michigan; the Department of Urology,¶ the First Affiliated Hospital, Sun Yat-Sen University, Guangzhou, China; and the Howard Hughes Medical Institute,** Ann Arbor, Michigan*

Accepted for publication November 19, 2013.

Address correspondence to Rohit Mehra, M.D., Department of Pathology, University of Michigan Health System, Room 2G332 UH, 1500 E Medical Center Dr, Ann Arbor, MI 48109. E-mail: mrohit@med.umich.edu.

Primary clear-cell adenocarcinoma of the urethra, a rare tumor that histomorphologically resembles clear-cell carcinoma of the female genital tract, occurs predominantly in women and is associated with a relatively poor prognosis. The histogenesis of this rare urethral neoplasm has not been completely resolved, but it is thought to arise from either müllerian rests or metaplastic urothelium. Herein, we present comprehensive surgical pathological and cytopathological findings from a patient with primary urethral clear-cell adenocarcinoma and describe next-generation sequencing results for this patient's unique tumor—the first such reported characterization of molecular aberrations in urethral clear-cell adenocarcinoma at the transcriptomic and genomic levels. Transcriptome analysis revealed novel gene fusion candidates, including *ANKRD28-FNDC3B*. Whole-exome analysis demonstrated focal copy number loss at the *SMAD4* and *ARID2* loci and 38 somatic mutations, including a truncating mutation in *ATM* and a novel nonsynonymous mutation in *ALK*. *(Am J Pathol 2014, 184: 584–591; http://dx.doi.org/10.1016/j.ajpath.2013.11.023)*

Primary carcinomas of the urethra are rare and, unlike most other genitourinary malignancies, occur more commonly in women than men.[1] In women, squamous cell carcinoma constitutes the vast majority of urethral carcinomas (approximately 70%), whereas conventional urothelial (transitional cell) carcinoma and conventional adenocarcinoma account for another 20% and 10%, respectively. There is a striking anatomical distribution of these tumors: distal urethral carcinomas are predominantly squamous cell type, whereas proximal urethral carcinomas are more often urothelial or adenocarcinoma type. Compared with other urinary tract malignancies, the prognosis for urethral carcinoma is poor, and patients often present with metastatic disease. The two principal prognostic factors for urethral carcinoma are pathological stage and tumor location, with a tendency for distal tumors (ie, squamous cell carcinoma) to have a better prognosis than proximal tumors (ie, urothelial carcinoma or adenocarcinoma).

Although rare variants have been reported, primary urethral adenocarcinoma generally shows either columnar/mucinous or clear-cell histomorphological features.[2] Columnar/mucinous adenocarcinoma resembles well-differentiated colonic or endocervical adenocarcinoma, whereas clear-cell adenocarcinoma is similar to clear-cell carcinoma of the female genital tract. In their seminal report, Oliva and Young[3] described the

This study was supported by the A. Alfred Taubman Medical Institute (A.M.C.), the American Cancer Society (A.M.C.), the Howard Hughes Medical Institute (A.M.C.), and a Doris Duke Charitable Foundation Clinical Scientist Award (A.M.C.); the National Center for Advancing Translational Sciences of the NIH under award KL2TR000434 (A.A.); and the Prostate Cancer Foundation (R.M. and A.M.C.) and National Human Genome Research Institute Clinical Sequencing Exploratory Research Consortium grant UM1HG006508 (R.M. and A.M.C.).

P.V. and S.K.-S. contributed equally to this work.

Disclosures: None declared.

http://dx.doi.org/10.1016/j.ajpath.2013.11.023

clinicopathological characteristics of a large cohort of primary urethral clear-cell adenocarcinomas. These tumors showed a marked sex predilection, with 18 cases in women compared with only 1 case in a man; in addition, most cases apparently arose within abnormally dilated periurethral structures—so-called urethral diverticula. Histomorphologically, these tumors displayed tubulocystic, papillary, and/or solid architecture and were composed of cells with clear cytoplasm, conspicuous nuclear atypia, and numerous mitotic figures.

The histogenesis of primary urethral clear-cell adenocarcinoma has not been conclusively determined. Although it was initially thought to arise from mesonephric remnants, the current hypothesis is that clear-cell adenocarcinoma derives from metaplastic urothelium or müllerian rests.[1,3–5] Alternative, but less widely accepted, theories include that the tumor originates from the periurethral (Skene's) glands or results from malignant transformation of nephrogenic adenoma.[6–8] The immunophenotype of this tumor reflects its histogenetic uncertainty.[2–4,7,9–13] Tumor cells usually express PAX8, cytokeratin (CK) 7, α-methylacyl-CoA racemase, HNF-1β, and high molecular weight cytokeratin (CK34βE12) proteins; there is often nuclear accumulation of p53; and the Ki-67 index is generally high (>25%). Tumor cells also show variable expression of CA-125 and CK20 but are routinely negative for prostate-specific antigen, estrogen receptor (ER), progesterone receptor (PR), and p63 protein expression. Although Sung et al[5] recently demonstrated frequent copy number gain of chromosomes 3, 7, and 17, similar to conventional urothelial carcinoma, by fluorescent *in situ* hybridization (FISH) in primary urethral clear-cell adenocarcinoma, little else is known about its molecular oncogenesis.

Herein, we present a patient with primary urethral clear-cell adenocarcinoma, detailing the relevant surgical pathological and cytopathological findings. We also describe next-generation sequencing results for this patient's tumor (the first such analysis of this type for primary urethral clear-cell adenocarcinoma), including several novel gene fusion candidates, copy number loss at the *SMAD4* and *ARID2* loci, and somatic mutations in *ATM* and *ALK*.

Materials and Methods

This study was approved by the University of Michigan (Ann Arbor) Health Sciences Institutional Review Board.

Immunohistochemistry

Immunohistochemistry (IHC) was performed by the Department of Pathology at the University of Michigan Health System using a BenchMark ULTRA automated stainer and the ultraView Universal DAB Detection Kit (Ventana Medical Systems, Oro Valley, AZ). The following primary antibodies were used: PAX8 (predilute; Cell Marque, Rocklin, CA), CK7 and CK20 (1:200; Cell Marque), and ER, PR, p63, and p53 (predilute; Ventana Medical Systems).

Sequencing and Mutation Analysis

Next-generation sequencing, including transcriptome, copy number, mutation, and gene fusion analysis, was performed as described previously.[14–17] Whole-exome and transcriptome sequencing was performed on a HiSeq 2000 (Illumina, San Diego, CA), and the resulting FASTQ sequence files were processed through in-house pipelines. For whole-exome sequencing, Novoalign Multithreaded software version 2.08.02 (Novocraft Technologies, Selangor, Malaysia) was used to align the sequencing reads to the human reference genome build (*hg19*/GRCh37). Mutation analysis was performed using VarScan 2 software version 2.3.2 (Washington University, St. Louis, MO),[18] and pileup files were produced by the SAMtools mpileup program.[19] Indel analysis was performed using Pindel, version 0.2.4 (Washington University),[20] and potential indel candidates were evaluated manually. Detected variants were functionally annotated using ANNOVAR.[21] For paired-end transcriptome sequencing, reads were aligned using Tophat2 software version 2.0.4 (University of Maryland, College Park, MD),[22] which internally deploys the ultrafast short read alignment algorithm Bowtie, version 0.12.8.[23] Junction reads supporting the fusion candidates were re-aligned with the BLAT alignment tool (UCSC Genome Bioinformatics, *http://genome.ucsc.edu/cgi-bin/hgBlat*, last accessed October 11, 2013) to confirm the predicted fusion breakpoint, and a full-length sequence of a fusion gene was constructed and evaluated for potential open reading frames (ORFs) using ORF Finder (National Center for Biotechnology Information, *http://www.ncbi.nlm.nih.gov/gorf/gorf.html*, last accessed October 11, 2013). Potential gene fusions with robust ORFs were explored using the Simple Modular Architecture Research Tool (*http://smart.embl-heidelberg.de*, last accessed October 11, 2013) to examine the gain or loss of known functional domains in the predicted fusion products.

Validation of Mutations and Fusions

For *ATM* somatic mutation validation, *ATM* exon 30 was PCR amplified from genomic DNA with sequence-specific primers (forward, 5′-M13-TGGCATATAAGAATTAGAGATGCT-GAA-3′; and reverse, 5′-TAACGTTGCGAACTGCTATCC-3′) and HotStart Taq DNA polymerase (Qiagen, Venlo, The Netherlands). The PCR product was purified with ExoSap-IT (Affymetrix, Santa Clara, CA) and subjected to Sanger sequencing at the University of Michigan DNA Sequencing Core using the M13 forward primer. Chromatograms were analyzed with Sequencher software version 4.5 (Gene Codes, Ann Arbor, MI).

For *ANKRD28-FNDC3B* gene fusion validation, total RNA was isolated from formalin-fixed, paraffin-embedded (FFPE) tissue samples using the miRNeasy FFPE Kit (Qiagen) and reverse transcribed using Superscript III (Life Technologies, Carlsbad, CA). PCRs were performed on a StepOne Real-Time PCR System (Life Technologies) with SYBR Green

dye and sequence-specific primers: *ANKRD28-FNDC3B* gene fusion transcript (forward, 5′-AACGGAGATCCTGATGAA-GTTCG-3′; and reverse, 5′-TAACACTCAGGAGACTGG-GGT-3′) and *GAPDH* internal control (forward, 5′-GT-CTCCTCTGACTTCAACAGCG-3′; and reverse, 5′-ACCA-CCCTGTTGCTGTAGCCAA-3′).

Results

Clinical History, Presentation, and Initial Work-Up

The patient is a 56-year-old African American woman with hepatitis C and uterine leiomyomata status post-hysterectomy (20 years prior), who presented for evaluation of abdominal pain and gross hematuria. In the patient's own words, her mother "nearly miscarried me twice in 1955, was hospitalized and treated with estrogens, possibly DES." From approximately 1940 to 1970, diethylstilbestrol (DES) was administered to pregnant women to reduce the risk of pregnancy complications and losses. In 1971, DES was shown to cause a clear-cell vaginal tumor in women exposed to this drug in utero. The US Food and Drug Administration subsequently banned the use of DES in pregnant women.

Eight years before the patient's presentation with hematuria, she had undergone bilateral salpingo-oophorectomy, which demonstrated a left ovarian serous cystadenoma and a right ovarian fibroma, but no ovarian cancer. On the most recent clinical evaluation, the patient was initially treated with antibiotics for a presumed urinary tract infection, without resolution of her symptoms. Follow-up studies demonstrated urinary retention, bladder atony, and right-sided hydronephrosis; urine cytological results were positive for atypical cells, which was interpreted as consistent with carcinoma, and reflex FISH testing with UroVysion showed a few cells with variable aneuploidy. The patient was subsequently referred for cystoscopic evaluation of a possible bladder tumor.

Cystoscopic Findings and TUR

On cystoscopy, a 2.5-cm sessile lesion of the posterior bladder wall was identified and completely resected. A separate large mass, involving approximately 60% of the urethra and apparently arising from within a diverticulum in the mid posterior urethral wall, was discovered and partially resected. Microscopic evaluation of the transurethral resection (TUR) specimens revealed fragments of tumor with predominantly papillary architecture (Figure 1A) and invasion into the lamina propria of the urethra. Separate fragments of partially denuded, reactive urothelium were identified, without evidence of urothelial dysplasia or conventional urothelial carcinoma. Tumor cells were medium sized, with distinct cell borders and vacuolated, clear cytoplasm; nuclei were basally located, medium sized, pleomorphic, and hyperchromatic, with irregular nuclear membranes, but without prominent nucleoli (Figure 1B). IHC demonstrated that the tumor cells diffusely and strongly expressed PAX8 and CK7 (Figure 1, C and D) but were negative for CK20, ER, PR, p53, and p63 protein expression (data not shown). The histomorphological features and immunophenotype were consistent with clear-cell adenocarcinoma. Repeat cystoscopy demonstrated residual tumor in the bladder and urethra, and restaging TUR showed muscle-invasive clear-cell adenocarcinoma with extension into the bladder neck.

Urine Cytopathological Findings

Concomitant with repeat cystoscopic examination, voided urine was obtained for cytopathological analysis; a ThinPrep slide (Hologic, Bedford, MA) was prepared and Papanicolaou stained. Microscopic examination revealed a cellular specimen composed predominantly of cohesive clusters of epithelial cells exhibiting overlapping nuclei with moderate to severe nuclear pleomorphism (Figure 2A). In areas, pleomorphic naked nuclei, singly and in loosely cohesive clusters, were also present (Figure 2B). The nuclei exhibited a delicate, vesicular to finely granular chromatin texture, and prominent nucleoli were occasionally encountered. Associated with some of the epithelial cell clusters, pseudohyphae and spore forms, consistent with *Candida* organisms, were visualized (Figure 2C). A cell block was prepared after pelleting the cellular material in the residual sample. H&E-stained sections, prepared from the cell block, revealed cohesive clusters of polygonal epithelial cells exhibiting vacuolated, clear cytoplasm (Figure 2D). Based on the constellation of findings, a diagnosis of clear-cell adenocarcinoma was confirmed.

Surgical and Pathological Findings following Anterior Pelvic Exenteration

Postcystoscopy magnetic resonance imaging of the abdomen and pelvis showed irregular posterior bladder wall thickening, from the level of the ureterovesical junction to the bladder neck and into the proximal urethra, consistent with postsurgical changes and probable residual tumor; limited separation of residual tumor from the anterior vaginal wall and bilateral pelvic lymphadenopathy were noted. A questionable 3-mm right upper lobe lung nodule was identified by computed tomography of the chest, but no other evidence of possible distant metastasis was detected. Overall, the cystoscopic, pathological, and radiological findings were consistent with a muscle-invasive primary urethral clear-cell adenocarcinoma with bladder neck involvement and regional lymph node metastasis. Given her pelvic pain, severe urinary symptoms, and uncertain response to systemic therapy, the patient elected to undergo anterior pelvic exenteration and bilateral pelvic lymph node dissection. Surgical pathological analysis of the resection specimen revealed a primary urethral clear-cell adenocarcinoma in the posterior wall of the proximal urethra, which grossly invaded the periurethral muscle into the periurethral and anterior vaginal soft tissue. The mass also extended superiorly through the bladder neck into the

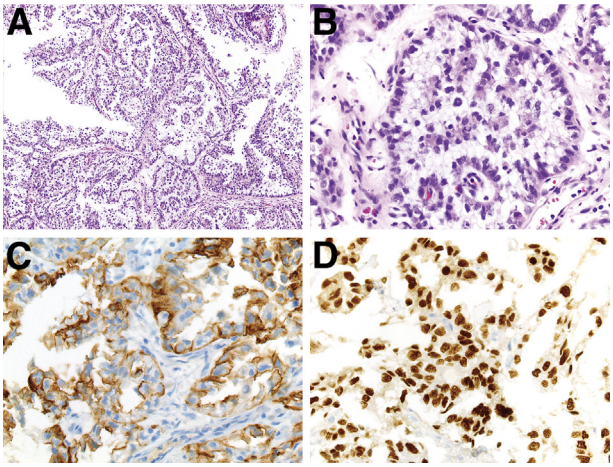

Figure 1 Histomorphological features and immunophenotype of a case of primary urethral clear-cell adenocarcinoma. **A** and **B:** H&E and IHC staining for CK7 (**C**) and PAX8 (**D**). **A:** The tumor showed a predominantly papillary architecture with fibrovascular septae and cores. **B:** Tumor cells had vacuolated, clear cytoplasm and basally located pleomorphic nuclei without prominent nucleoli. IHC demonstrated that tumor cells diffusely and strongly expressed CK7 in a membranous pattern (**C**) and PAX8 in a nuclear manner (**D**). Original magnification: ×100 (**A**); ×400 (**B**–**D**).

bladder trigone, with invasion of the bladder wall muscle and extension into the perivesicular adipose tissue. The soft tissue resection margin was negative for carcinoma. Five of eight pelvic lymph nodes were involved by metastatic clear-cell adenocarcinoma. Taken together, the pathological staging of our patient's tumor was pT4N2, which corresponds to clinical stage IV.[24]

Next-Generation Sequencing

Representative samples from FFPE tissue were selected for next-generation sequencing. Copy number analysis revealed several areas of copy number gain in tumor cells, including a region of 7q11.21 containing *TMEM248*, *SBDS*, and *TYW1* (log2 ratio = 1.25); a region of 8q13.2 containing *CPA6* and *PREX2* (log2 ratio = 1.13); a region of 8q21.3 containing *RIPK2*, *OSGIN2*, *DECR1*, and *CALB1* (log2 ratio = 1.10 to 1.51); a region of 20q13.33 containing *SS18L1* and *GTPBP5* (log2 ratio = 1.29); and a region of 22q13.2 containing *TEF*, *TOB2*, *PHF5A*, *ACO2*, *POLR3H*, and *PMM1* (log2 ratio = 1.32 to 2.08) (Figure 3A and Supplemental Table S1). In addition, there was copy number loss of a region of 12q12 containing *ARID2* (log2 ratio = −1.41) and an area of focal copy number loss on 18q21.2 containing *SMAD4* (log2 ratio = −0.98) (Figure 3, A and F).

Mutation analysis revealed 38 somatic point mutations, including a nonsense mutation in *ATM* and a novel nonsynonymous mutation of unknown significance in *ALK* (Supplemental Tables S2 and S3). A cytosine to thymine transition in exon 30 of *ATM* generates a premature stop codon at amino acid position 1537; the predicted truncated ATM protein lacks the critical C-terminal FAT and phosphatidylinositol 3-kinase catalytic (PI3KC) domains (Figure 3B). This somatic mutation in *ATM* was independently validated by Sanger sequencing (Figure 3C). In the *ALK* gene, a thymine to guanine transversion in exon 19 results in substitution of proline for threonine at amino acid position 1026; this amino acid change occurs N-terminal to the ALK tyrosine kinase domain, in a region without well-characterized functional domains. Finally, a single-nucleotide somatic insertion of thymine in exon 10 of *ATR* results in a premature stop codon at amino acid position 775 and, similar to the *ATM* nonsense mutation, yields a truncated ATR protein without the FAT or PI3KC domains; this *ATR* indel, however, could not be independently validated by Sanger sequencing.

Transcriptome analysis identified 104 gene fusion candidates (Supplemental Table S4), five of which were considered true-positive candidates by subsequent manual curation: *ANKRD28-FNDC3B*, *RIPK2-OSGIN2*, *PDLIM1-LOC728558*, *HMGA2-EML5*, and *RB1-SLC15A2* (Supplemental Table S4). The *ANKRD28-FNDC3B* gene fusion results from an intrachromosomal rearrangement of chromosome 3, which joins exon 2 of *ANKRD28* to exon 4 of *FNDC3B*. The predicted fusion protein contains most of the C-terminal portion of FNDC3B, with nine fibronectin type III domains and a single transmembrane domain (Figure 3D). This *ANKRD28-FNDC3B* fusion transcript was independently validated by quantitative PCR analysis (Figure 3E). The *RIPK2-OSGIN2* gene fusion is found in a region of copy number gain; it results from an intrachromosomal rearrangement of chromosome 8, which joins the last five exons of *RIPK2* to the 3′ untranslated region of *OSGIN2*. The *PDLIM1-LOC728558* gene fusion results from an intrachromosomal rearrangement of chromosome 10, which fuses exon 1 of *PDLIM1* to an anti-sense, noncoding

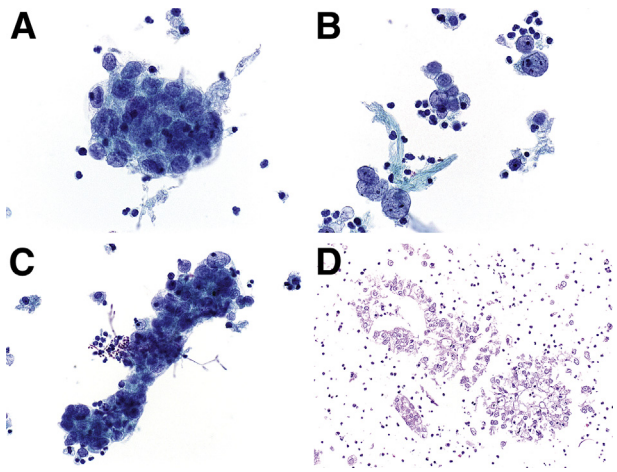

Figure 2 Cytomorphological findings of a voided urine specimen in a case of primary urethral clear-cell adenocarcinoma. **A**–**C:** Papanicolaou-stained ThinPrep slides. A voided urine specimen contained cohesive, three-dimensional clusters of epithelial cells with moderate to severe nuclear pleomorphism (**A**); pleomorphic, naked nuclei with delicate, finely granular chromatin texture and occasionally prominent nucleoli (**B**); and fungal spore forms and pseudohyphae, consistent with *Candida* organisms, intimately associated with elongated epithelial cell clusters (**C**). **D:** A cell block section demonstrated clusters of polygonal epithelial cells with clear cytoplasm (H&E stain). Original magnification: ×600 (**A**–**C**); ×400 (**D**).

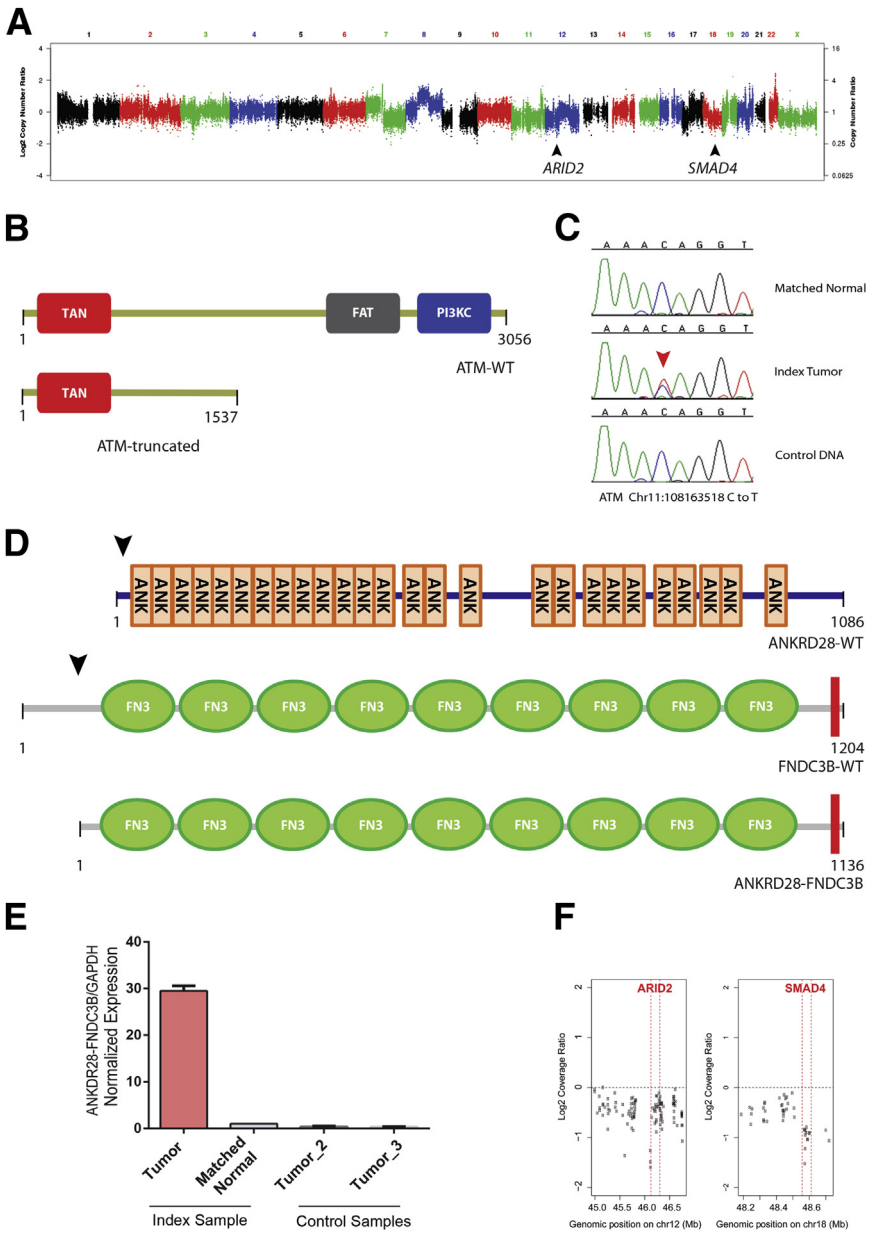

Figure 3 Next-generation sequencing of a case of primary urethral clear-cell adenocarcinoma. **A:** Copy number analysis demonstrated several regions of copy number gain, as well as copy number loss at 12q12 and 18q21.1, which contain the *ARID2* and *SMAD4* loci (**black arrowheads**), respectively: *y* axis = log2 transformed tumor-to-normal coverage ratio; and *x* axis = genomic position, ascending from left to right (chromosome number depicted above). **B:** Mutation analysis revealed a truncating somatic mutation in *ATM*, which results in a premature stop codon at amino acid position 1537; the truncated ATM protein is missing the FAT and PI3KC domains. **C:** Sanger sequencing validation of this *ATM* somatic mutation demonstrates a C-to-T nucleotide transition at chr11:108163518 in the tumor sample but not matched normal or control human genomic DNA. **D:** A novel *ANKRD28-FNDC3B* gene fusion. Wild-type ANKRD28 protein (ANKRD28-WT) contains 26 ankyrin repeats (ANK), and wild-type FNDC3B protein (FNDC3B-WT) contains nine type fibronectin type III domains (FN3) and a single C-terminal transmembrane domain (**red box**). The *ANKRD28-FNDC3B* gene fusion transcript joins the N-terminal portion of *ANKRD28* and the C-terminal portion of *FNDC3B* (**black arrows**), generating a predicted translated peptide that contains only the FN3 and transmembrane domains of FNDC3B (ANKRD28-FNDC3B). **E:** Quantitative PCR validation of this *ANKRD28-FNDC3B* gene fusion. All expression values are normalized to the internal control *GAPDH*. **F:** High resolution of copy number losses at *ARID2* and *SMAD4*: *y* axis, log2 transformed tumor-to-normal coverage ratio; and *x* axis, genomic position (in Mb), with each point representing a targeted exon and respective gene boundaries being highlighted by red vertical lines.

RNA within the *ENTPD1* locus. The *HMGA2-EML5* gene fusion results from a translocation between 12q14.3 and 14q31.3, which joins the first three exons of *HMGA2* to the last 18 exons of *EML5* (exons 27 to 44). The *RB1-SLC15A2* gene fusion results from a translocation between 3q13.33 and 13q14.2, which joins the first 19 exons of *RB1* to the last 13 exons of *SLC15A2* (exons 10 to 22).

Clinical Follow-Up

A computed tomographic scan of the abdomen and thorax 2 months postoperatively showed no evidence of residual or metastatic disease. Given the high pathological stage and regional lymph node metastases, however, adjuvant radiation and chemotherapy were recommended, and the patient received two cycles of systemic cisplatin and approximately 48.2 Gy of radiation to the pelvis. At latest follow-up, 11 months after surgery, the patient was alive without evidence of tumor recurrence.

Discussion

Primary urethral clear-cell adenocarcinoma is a rare, aggressive tumor that poses a difficult diagnostic challenge for pathologists and a therapeutic question for urologists. The differential diagnosis for urethral clear-cell lesions includes metastatic clear-cell carcinoma of the female genital tract, urothelial carcinoma with clear-cell features or tubulocystic architecture, metastatic clear-cell renal cell carcinoma (RCC), and nephrogenic adenoma.[1] Distinguishing

primary urethral clear-cell adenocarcinoma from urothelial carcinoma or metastatic clear-cell RCC is usually possible based on histomorphological characteristics (eg, the presence of conventional urothelial carcinoma) and/or a limited panel of IHC stains, including p63 (positive in urothelial carcinoma) and CK7 (negative in clear-cell RCC). Although nephrogenic adenoma can be a close histological and immunophenotypic mimic of primary urethral clear-cell adenocarcinoma,[10,25] these two entities can usually be distinguished on clinicoradiological grounds (eg, large mass on cystoscopy or radiological evidence of regional or distant metastasis) or by close pathological assessment.

Our patient's case highlights the histogenetic uncertainty of primary urethral clear-cell adenocarcinoma. The prevailing theories suggest that these tumors arise from either müllerian rests or metaplastic urothelium.[1,3–5] Although our patient's tumor would be consistent with either of these possibilities, because of its association with an apparent urethral diverticulum, we favor that it most likely arose from metaplastic urothelium. Urethral diverticula lead to urinary stasis, which can result in recurrent urinary tract infections or calculus formation.[26] Similar to other areas of the urinary tract, the resulting chronic irritation and inflammation can predispose to malignant transformation. Although no müllerian rests were identified in the TUR biopsy specimens or main surgical specimen, the immunophenotype and location of the tumor in the proximal posterior urethra suggest that a müllerian origin cannot be completely excluded.

In addition to the surgical pathological findings of her primary tumor, we have described cytopathological results from a sample of our patient's voided urine. The cytological specimen demonstrated clusters of cohesive, vacuolated epithelial cells with pleomorphic, vesicular nuclei and prominent nucleoli, and the cell block specimen closely resembled the tumor histomorphological characteristics in the TUR (Figure 2). Although relatively few studies have examined the cytopathological features of primary urethra clear-cell adenocarcinoma, the reported cytomorphological features are similar to our patient's case, and cell block IHC for PAX8, p63, CK7, CK20, p53, and Ki-67 may help to discriminate between different urethral clear-cell lesions.[13,27,28] These data suggest that, when sufficient materials are not available by TUR biopsy specimen, urine cytopathological analysis may be useful for the accurate diagnosis of clear-cell adenocarcinoma.

The molecular oncogenesis of primary urethral clear-cell adenocarcinoma is not well understood. To investigate possible molecular mechanisms underlying tumorigenesis of our patient's unique cancer, we performed transcriptome, copy number, and mutation analyses by next-generation sequencing—the first such analysis for primary urethral clear-cell adenocarcinoma. A recent report described FISH analysis of primary urethral clear-cell adenocarcinoma and showed frequent copy number gain of chromosomes 3, 7, and 17, a pattern similar to conventional urothelial carcinoma.[5] In contrast, analysis of our patient's tumor by next-generation sequencing demonstrated copy number gain of chromosomes 7, 8, 20, and 22. The reason for this discordance is unclear but may be the result of low sample size, tumor heterogeneity, and/or differences in technique. Interestingly, amplification of chromosome 8 included the *PREX2* locus, a gene encoding a guanine nucleotide exchange factor whose overexpression is associated with inhibition of PTEN activity.[29] Focal copy number loss at the *SMAD4* locus on chromosome 22 was also detected. *SMAD4* encodes a key intracellular protein in the bone morphogenetic protein signaling pathway and functions as a tumor suppressor in a variety of human cancers, most notably pancreatic and colon cancers.[30] *SMAD4* loss of heterozygosity is frequently observed in these cancer types, and germ-line *SMAD4* heterozygosity underlies juvenile polyposis syndrome, a rare autosomal dominant disorder characterized by hamartomatous polyps and tumors of the gastrointestinal tract. Finally, we detected copy number loss at the *ARID2* locus on chromosome 12. *ARID2* encodes a DNA-binding protein involved in the specificity of chromatin remodeling by SWItch/sucrose nonfermentable (SWI/SNF) complexes, and recurrent inactivating somatic mutations in *ARID2* have been detected in a range of human cancers, including hepatocellular carcinoma, pancreatic ductal adenocarcinoma, melanoma, and non-small cell lung carcinoma.[31–33]

Mutation analysis revealed 38 somatic alterations in the exome, including a truncating *ATM* mutation and a novel nonsynonymous *ALK* mutation. The phosphoinositide 3-kinase-related kinase subfamily member ATM is a protein kinase with a well-recognized role in the cellular response to DNA damage via activation of cell cycle checkpoints and acts as a tumor suppressor in a variety of human cancers.[34] The nonsense *ATM* mutation results in a truncated ATM protein (ie, without the FAT3 and PI3KC functional domains), which leads to the disruption of the ATM-mediated DNA damage response pathway. This is interesting in light of the lack of nuclear p53 accumulation in our patient's tumor, which is otherwise a common IHC feature of primary urethral clear-cell adenocarcinomas. Nuclear p53 expression in tumor cells usually results from the accumulation of undegraded mutant p53 after somatic alteration of *TP53*. Thus, the absence of nuclear p53 accumulation in our patient's tumor suggests an intact *TP53* gene, which is concordant with our next-generation sequencing results. *ATM* and *TP53* function together in the DNA damage response pathway, and interestingly, a negative correlation between *ATM* and *TP53* mutations has been reported in a large cohort of sequenced lung adenocarcinomas.[35] This suggests that mutation of *ATM* in our patient's tumor may be sufficient for dysregulation of the DNA damage response pathway. Finally, a nonsynonymous mutation of unknown significance was detected in the ligand-binding domain of the orphan nuclear receptor transcription factor *NR5A2*; interestingly, recent genome-wide association studies have linked this gene locus to susceptibility for pancreatic ductal adenocarcinoma.[36]

Transcriptome analysis identified the novel gene fusion candidate *ANKRD28-FNDC3B*. This gene fusion joins exon 2 of *ANKRD28* to exon 4 of *FNDC3B* and generates an essentially intact FNDC3B protein under aberrant transcriptional control of the *ANKRD28* regulatory regions (Figure 3D). *FNDC3B* is present on chromosome 3q26, which is frequently amplified in a diverse number of human cancer types, and overexpression of *FNDC3B* has been implicated in epithelial-to-mesenchymal transition and activation of an array of cellular signaling pathways, including retinoblastoma, phosphoinositide 3-kinase, and mitogen-activated protein kinase/extracellular signal–regulated kinase.[37] In hepatocellular carcinoma, for example, *FNDC3B* amplification and aberrant up-regulation promote cellular proliferation via activation of the STAT3 signaling pathway.[38]

In summary, we have described the surgical pathological, cytopathological, and molecular pathological findings from a patient with primary urethral clear-cell adenocarcinoma. Our patient's tumor demonstrated many of the classic clinical and histomorphological features of this rare, aggressive cancer, and the urine cytopathological results were concordant with emerging data in the scientific literature. Next-generation sequencing revealed a fount of novel data about the possible molecular underpinnings of this unique cancer type, including dysregulation of DNA damage response (*ATM*) and chromatin remodeling (*ARID2*) and changes in signaling pathways (*PREX2*, *SMAD4*, and *ANKRD28-FNDC3B*). These molecular data highlight the possibility of emerging clinical/therapeutic approaches to rare tumors in the current era of personalized medicine and provide exciting new opportunities to explore the molecular oncogenesis of primary urethral clear-cell adenocarcinoma. Follow-up studies with a larger cohort of tumors could analyze molecular differences between clear-cell tumors of the urinary and female genital tracts or investigate the as-of-yet unresolved issue of the histogenesis of primary urethral clear-cell adenocarcinoma.

Acknowledgments

We thank Tina Fields and the histology staff [Department of Pathology, University of Michigan (Ann Arbor) Health System] for technical assistance and Karen Giles for assistance with manuscript submission.

Supplemental Data

Supplemental material for this article can be found at *http://dx.doi.org/10.1016/j.ajpath.2013.11.023*.

References

1. Amin MB, Young RH: Primary carcinomas of the urethra. Semin Diagn Pathol 1997, 14:147–160
2. Meis JM, Ayala AG, Johnson DE: Adenocarcinoma of the urethra in women: a clinicopathologic study. Cancer 1987, 60:1038–1052
3. Oliva E, Young RH: Clear cell adenocarcinoma of the urethra: a clinicopathologic analysis of 19 cases. Mod Pathol 1996, 9:513–520
4. Drew PA, Murphy WM, Civantos F, Speights VO: The histogenesis of clear cell adenocarcinoma of the lower urinary tract: case series and review of the literature. Hum Pathol 1996, 27:248–252
5. Sung MT, Zhang S, MacLennan GT, Lopez-Beltran A, Montironi R, Wang M, Tan PH, Cheng L: Histogenesis of clear cell adenocarcinoma in the urinary tract: evidence of urothelial origin. Clin Cancer Res 2008, 14:1947–1955
6. Spencer JR, Brodin AG, Ignatoff JM: Clear cell adenocarcinoma of the urethra: evidence for origin within paraurethral ducts. J Urol 1990, 143:122–125
7. Tong GX, Weeden EM, Hamele-Bena D, Huan Y, Unger P, Memeo L, O'Toole K: Expression of PAX8 in nephrogenic adenoma and clear cell adenocarcinoma of the lower urinary tract: evidence of related histogenesis? Am J Surg Pathol 2008, 32:1380–1387
8. Reis LO, Billis A, Ferreira FT, Ikari LY, Stellini RF, Ferreira U: Female urethral carcinoma: evidences to origin from Skene's glands. Urol Oncol 2011, 29:218–223
9. Dodson MK, Cliby WA, Pettavel PP, Keeney GL, Podratz KC: Female urethral adenocarcinoma: evidence for more than one tissue of origin? Gynecol Oncol 1995, 59:352–357
10. Gilcrease MZ, Delgado R, Vuitch F, Albores-Saavedra J: Clear cell adenocarcinoma and nephrogenic adenoma of the urethra and urinary bladder: a histopathologic and immunohistochemical comparison. Hum Pathol 1998, 29:1451–1456
11. Sun K, Huan Y, Unger PD: Clear cell adenocarcinoma of urinary bladder and urethra: another urinary tract lesion immunoreactive for P504S. Arch Pathol Lab Med 2008, 132:1417–1422
12. Brimo F, Herawi M, Sharma R, Netto GJ, Epstein JI, Illei PB: Hepatocyte nuclear factor-1beta expression in clear cell adenocarcinomas of the bladder and urethra: diagnostic utility and implications for histogenesis. Hum Pathol 2011, 42:1613–1619
13. Alexiev BA, Tavora F: Histology and immunohistochemistry of clear cell adenocarcinoma of the urethra: histogenesis and diagnostic problems. Virchows Arch 2013, 462:193–201
14. Roychowdhury S, Iyer MK, Robinson DR, Lonigro RJ, Wu YM, Cao X, Kalyana-Sundaram S, Sam L, Balbin OA, Quist MJ, Barrette T, Everett J, Siddiqui J, Kunju LP, Navone N, Araujo JC, Troncoso P, Logothetis CJ, Innis JW, Smith DC, Lao CD, Kim SY, Roberts JS, Gruber SB, Pienta KJ, Talpaz M, Chinnaiyan AM: Personalized oncology through integrative high-throughput sequencing: a pilot study. Sci Transl Med 2011, 3:111ra121
15. Robinson DR, Wu YM, Kalyana-Sundaram S, Cao X, Lonigro RJ, Sung YS, Chen CL, Zhang L, Wang R, Su F, Iyer MK, Roychowdhury S, Siddiqui J, Pienta KJ, Kunju LP, Talpaz M, Mosquera JM, Singer S, Schuetze SM, Antonescu CR, Chinnaiyan AM: Identification of recurrent NAB2-STAT6 gene fusions in solitary fibrous tumor by integrative sequencing. Nat Genet 2013, 45:180–185
16. Roychowdhury S, Chinnaiyan AM: Advancing precision medicine for prostate cancer through genomics. J Clin Oncol 2013, 31:1866–1873
17. Wu YM, Su F, Kalyana-Sundaram S, Khazanov N, Ateeq B, Cao X, Lonigro RJ, Vats P, Wang R, Lin SF, Cheng AJ, Kunju LP, Siddiqui J, Tomlins SA, Wyngaard P, Sadis S, Roychowdhury S, Hussain MH, Feng FY, Zalupski MM, Talpaz M, Pienta KJ, Rhodes DR, Robinson DR, Chinnaiyan AM: Identification of targetable FGFR gene fusions in diverse cancers. Cancer Discov 2013, 3:636–647
18. Koboldt DC, Zhang Q, Larson DE, Shen D, McLellan MD, Lin L, Miller CA, Mardis ER, Ding L, Wilson RK: VarScan 2: somatic mutation and copy number alteration discovery in cancer by exome sequencing. Genome Res 2012, 22:568–576
19. Li H, Handsaker B, Wysoker A, Fennell T, Ruan J, Homer N, Marth G, Abecasis G, Durbin R: The Sequence Alignment/Map format and SAMtools. Bioinformatics 2009, 25:2078–2079

20. Ye K, Schulz MH, Long Q, Apweiler R, Ning Z: Pindel: a pattern growth approach to detect break points of large deletions and medium sized insertions from paired-end short reads. Bioinformatics 2009, 25: 2865−2871
21. Wang K, Li M, Hakonarson H: ANNOVAR: functional annotation of genetic variants from high-throughput sequencing data. Nucleic Acids Res 2010, 38:e164
22. Kim D, Pertea G, Trapnell C, Pimentel H, Kelley R, Salzberg SL: TopHat2: accurate alignment of transcriptomes in the presence of insertions, deletions and gene fusions. Genome Biol 2013, 14:R36
23. Langmead B, Trapnell C, Pop M, Salzberg SL: Ultrafast and memory-efficient alignment of short DNA sequences to the human genome. Genome Biol 2009, 10:R25
24. Edge SB American Joint Committee on Cancer: AJCC Cancer Staging Manual. New York, Springer, 2010, pp 648
25. Herawi M, Drew PA, Pan CC, Epstein JI: Clear cell adenocarcinoma of the bladder and urethra: cases diffusely mimicking nephrogenic adenoma. Hum Pathol 2010, 41:594−601
26. Patel AK, Chapple CR: Female urethral diverticula. Curr Opin Urol 2006, 16:248−254
27. Nakatsuka S, Taguchi I, Nagatomo T, Yamane M, Sugio K, Yoshino R, Oku K, Nagano T, Kimura H, Nakajo K, Kawabata G: A case of clear cell adenocarcinoma arising from the urethral diverticulum: utility of urinary cytology and immunohistochemistry. Cytojournal 2012, 9:11
28. Doria MI Jr., Saint Martin G, Wang HH, Blumstein A, Jensen JA, Maslan AM, Gattuso P: Cytologic features of clear cell carcinoma of the urethra and urinary bladder. Diagn Cytopathol 1996, 14:150−154
29. Fine B, Hodakoski C, Koujak S, Su T, Saal LH, Maurer M, Hopkins B, Keniry M, Sulis ML, Mense S, Hibshoosh H, Parsons R: Activation of the PI3K pathway in cancer through inhibition of PTEN by exchange factor P-REX2a. Science 2009, 325:1261−1265
30. Yang G, Yang X: Smad4-mediated TGF-beta signaling in tumorigenesis. Int J Biol Sci 2010, 6:1−8
31. Shain AH, Pollack JR: The spectrum of SWI/SNF mutations, ubiquitous in human cancers. PLoS One 2013, 8:e55119
32. Manceau G, Letouze E, Guichard C, Didelot A, Cazes A, Corte H, Fabre E, Pallier K, Imbeaud S, Le Pimpec-Barthes F, Zucman-Rossi J, Laurent-Puig P, Blons H: Recurrent inactivating mutations of ARID2 in non-small cell lung carcinoma. Int J Cancer 2013, 132:2217−2221
33. Biankin AV, Waddell N, Kassahn KS, Gingras MC, Muthuswamy LB, Johns AL, et al: Pancreatic cancer genomes reveal aberrations in axon guidance pathway genes. Nature 2012, 491:399−405
34. Nam EA, Cortez D: ATR signalling: more than meeting at the fork. Biochem J 2011, 436:527−536
35. Ding L, Getz G, Wheeler DA, Mardis ER, McLellan MD, Cibulskis K, et al: Somatic mutations affect key pathways in lung adenocarcinoma. Nature 2008, 455:1069−1075
36. Petersen GM, Amundadottir L, Fuchs CS, Kraft P, Stolzenberg-Solomon RZ, Jacobs KB, et al: A genome-wide association study identifies pancreatic cancer susceptibility loci on chromosomes 13q22.1, 1q32.1 and 5p15.33. Nat Genet 2010, 42:224−228
37. Cai C, Rajaram M, Zhou X, Liu Q, Marchica J, Li J, Powers RS: Activation of multiple cancer pathways and tumor maintenance function of the 3q amplified oncogene FNDC3B. Cell Cycle 2012, 11:1773−1781
38. Chen CF, Hsu EC, Lin KT, Tu PH, Chang HW, Lin CH, Chen YJ, Gu DL, Wu JY, Chen YT, Hsu MT, Jou YS: Overlapping high-resolution copy number alterations in cancer genomes identified putative cancer genes in hepatocellular carcinoma. Hepatology 2010, 52: 1690−1701